

Linear Scaling Real Time TDDFT in the ConQuEST Code

Conn O'Rourke^{*,†,‡,¶} and David R. Bowler^{†,‡,¶}

London Centre for Nanotechnology, 17-19 Gordon St, London, WC1H 0AH, Department of Physics & Astronomy, University College London, Gower St, London, WC1E 6BT, and UCL Satellite, International Centre for Materials Nanoarchitectonics (MANA), National Institute for Materials Science (NIMS), 1-1 Namiki, Tsukuba, Ibaraki 305-0044, Japan

E-mail: ucapcor@live.ucl.ac.uk

Abstract

Density matrix based, real-time time dependent density functional theory (RT-TDDFT) has been implemented in the linear scaling density functional theory code CONQUEST. Imposing a spatial cut-off radius on the density matrix allows the computational workload to be made to scale linearly with system size. In this paper, following an illustration of the soundness of our implementation, we go on to discuss how imposing these spatial cut-offs affect the propagation. In particular we show the effect on the unitarity of the real-time density matrix propagator of the spatial cut-offs, the propagation time step and the matrix exponential approximations. Finally we discuss the effect of density matrix truncation on the generated optical spectra for long chain alkane molecules, and illustrate that imposing these cut-offs allows the computational time to scale linearly with system size without compromising efficiency.

*To whom correspondence should be addressed

[†]LCN

[‡]UCL

[¶]UCL Satellite, MANA

1 Introduction

Density functional theory (DFT) has become an almost ubiquitous tool in the arsenal of the electronic structure theorist^{1,2}. Extending DFT to the time domain results in its excited state counterpart, time dependent density functional theory (TDDFT)^{3,4}.

Casida’s linear response formulation of TDDFT⁵ (LR-TDDFT) requires the solution of an eigenvalue equation for a matrix Ω written in the space of electron-hole pairs, which scales poorly with system size $\sim \mathcal{O}(N^6)$, where N is the number of atoms. However, in effect, this scaling can be reduced through efficient implementations of Casida’s LR-TDDFT, and alternative methods employing the Liouville-Lanczos approach which have significantly reduced this scaling as far as $\mathcal{O}(N^3)$ ^{6,7}.

Real time propagation of the time-dependent Kohn-Sham equations, pioneered by Yabana and Bertsch⁸, provides an alternative approach to Casida’s linear response formalism and associated methods. Real time TDDFT (RT-TDDFT) proceeds by the construction of an effective Hamiltonian, followed by the direct propagation of the Kohn-Sham orbitals using this Hamiltonian. Assuming both the number of occupied states (N_{KS}) and the number of mesh points (N_M) scale linearly with system size, RT-TDDFT will scale with the number of atoms, N , as $N_{KS}N_M \sim N^2$. A significant prefactor in the form of the number of time steps and the computational effort for construction of the Hamiltonian exists, making this method unsuitable for systems of small size. However the $\mathcal{O}(N^2)$ scaling have made it the natural choice for tackling systems of large size, and a complementary partner to Casida’s approach.

Linear scaling, or $\mathcal{O}(N)$, density functional theory is now well established⁹. In a similar manner the computational workload of RT-TDDFT based on the propagation of the density matrix, as opposed to the Kohn-Sham orbitals, can be made to scale *linearly* with system size. Reductions in the computational expense obtained by working with the truncated density matrix open up the possibility of studying excited states in large systems that cannot feasibly be examined with other methods.

RT-TDDFT based on density matrix propagation has been used to study fullerene, sodium

clusters, polyacetylene oligomers, carbon nanotubes and silicon clusters to name a few^{10–16}, and has been shown to scale linearly with system size. It is also worth noting that linear scaling density matrix based LR-TDDFT, avoiding the propagation of the density matrix, has also been recently demonstrated¹⁷.

In this paper we very briefly summarize our implementation of RT-TDDFT in the CONQUEST code and confirm the reliability of the implementation. We then present tests on the limits of the method, and the factors affecting accuracy. In particular we examine the effect of matrix truncation, the key approximation used in achieving linear scaling, on the unitarity of the propagators used and optical spectra generated.

2 Computational Approach

2.1 Linear Scaling DFT & RT-TDDFT

Linear scaling density functional theory is now well established (for a review see⁹), with the central idea to exploit the principle of nearsightedness¹⁸ of electron interactions in some way to reduce the computational workload. Rather than working with the conventional single particle Kohn-Sham orbitals, CONQUEST works with the density matrix written in a separable form in terms of a localised basis of support functions $\phi_{i\alpha}$

$$\rho(\mathbf{r}, \mathbf{r}') = \sum_{i\alpha, j\beta} \phi_{i\alpha}(\mathbf{r}) K_{i\alpha, j\beta} \phi_{j\beta}(\mathbf{r}') \quad (1)$$

where $\phi_{i\alpha}$ is the α^{th} support function centred on atom i . Support functions are a non-orthogonal basis set of localised orbitals, and have an overlap matrix given by:

$$\mathbf{S}_{\alpha, \beta} = \int \phi_{i\alpha}(\mathbf{r}) \phi_{j\beta}(\mathbf{r}) d\mathbf{r} \quad (2)$$

Linear scaling behaviour can be obtained through applying a spatial cut-off on the density matrix. Beyond this cut-off radius the matrix elements are set to zero which, along with the spatial

limitation of the support functions, ensures that the number of non-zero density matrix elements increases linearly with system size (for a fuller overview of the CONQUEST code see¹⁹).

Diagonalisation or orthogonalisation of Kohn-Sham eigenfunctions in conventional DFT methods intrinsically scales as $\mathcal{O}(N^3)$, providing a computational bottleneck which limits system size. $\mathcal{O}(N)$ methods do not suffer from the same bottleneck, allowing vastly larger systems to be studied. For example Conquest has been used to perform calculations on millions of atoms²⁰.

Similarly RT-TDDFT is now well established⁸, and implementations of density matrix RT-TDDFT have previously been discussed^{21,22}. Rather than employing an orthogonalisation procedure via a Cholesky or Löwdin decomposition, as is done elsewhere, we work in our non-orthogonal basis. Expanding the time-dependent Kohn-Sham equations in this basis of non-orthogonal support functions, in the instance where the support functions are stationary with time, gives

$$i\frac{\partial}{\partial t}\mathbf{c}(t) = \mathbf{S}^{-1}\mathbf{H}\mathbf{c}(t) \quad (3)$$

and

$$i\frac{\partial}{\partial t}\mathbf{c}^\dagger(t) = -\mathbf{c}^\dagger(t)\mathbf{H}\mathbf{S}^{-1} \quad (4)$$

which describe the time dependence of the coefficients of our basis set expansion, $\mathbf{c}(t)$. This allows us to write the quantum Liouville equation of motion for our auxiliary density matrix \mathbf{K} in the non-orthogonal support function basis:

$$i\dot{\mathbf{K}} = \mathbf{S}^{-1}\mathbf{H}\mathbf{K} - \mathbf{K}\mathbf{H}\mathbf{S}^{-1} \quad (5)$$

The formal solution to this equation can be expressed as:

$$\mathbf{K}(t) = \mathbf{U}(t, t_0)\mathbf{K}(t_0)\mathbf{U}^\dagger(t_0, t) \quad (6)$$

where $\mathbf{U}(t, t_0)$ is a propagator satisfying both:

$$\mathbf{c}(\mathbf{t}) = \mathbf{U}(t, t_0)\mathbf{c}(t_0) \quad (7)$$

$$i\frac{\partial}{\partial t}\mathbf{U}(t, t_0) = \mathbf{S}^{-1}\mathbf{H}\mathbf{U}(t, t_0) \quad (8)$$

Expressing the propagator in integral form we have:

$$\mathbf{U}(t, t_0) = \mathcal{T} \exp \left\{ -i \int_{t_0}^t d\tau \mathbf{S}^{-1} \mathbf{H}(\tau) \right\} \quad (9)$$

where \mathcal{T} is the time ordering operator. Evolution of the system for a total time, $T = n\Delta t$, may be carried out piecewise in smaller intervals, allowing us to express the total evolution operator as the product of small time operators:

$$\mathbf{U}(t, t_0) \simeq \prod_{n=0}^{N-1} \mathbf{U}((n+1)\Delta t, n\Delta t) \quad (10)$$

where

$$\mathbf{U}(t + \Delta t, t) = \exp \left[-i\mathbf{S}^{-1} \mathbf{H}(\tau) \Delta t \right] \quad (11)$$

Evolution of the time dependent system is then reduced to the problem of approximating the propagator $\mathbf{U}(t + \Delta t, t)$. Two approximations exist in the definition of $\mathbf{U}(t + \Delta t, t)$, firstly that of approximating the matrix exponential $\exp(\mathbf{A})$ and secondly the exact form of the matrix for which we wish to calculate the exponential. There are several methods for calculating the exponential of a matrix²³, here we use the simplest approximation, a Taylor expansion:

$$\exp(\mathbf{A}\Delta t) = \mathbf{I} + \sum_{n=1}^{\infty} \frac{(\mathbf{A}\Delta t)^n}{n!} \quad (12)$$

Similarly there are many different approaches for deciding which matrix exponential to use as

a propagator. Three approximations have been implemented: the so called *exponential-midpoint* propagator (EM), the *enforced time-reversal symmetry* (ETRS) propagator and the fourth order Magnus (M4) propagators, all of which are taken from the work of Marques et al.²⁴ on RT-TDDFT propagators. We briefly describe these propagators written in our non-orthogonal basis in supporting information for completeness (SI1).

Propagating the density matrix in real time in this manner provides direct access to the time dependent charge density, and therefore the electronic response to external electric fields. The polarisability of the system under study can then be calculated, and is directly proportional to the experimentally measured absorption strength function. This idea behind extracting optical transitions from the linear response of a system to an external electric field is well known^{8,25}, but we have included a brief description of the procedure along with an illustration of the response of a benzene molecule in supporting information (SI2).

2.2 Small Molecules

In order to verify that our implementation is correct we have performed tests on several systems for which the electronic transitions have been studied experimentally and theoretically elsewhere, allowing us to make direct comparisons. For this purpose we have chosen four small molecules (Carbon monoxide, Methane, Ethylene and Benzene) and used our implementation to calculate the optical absorption spectra within the TDLDA approximation.

Meaningful comparison of our results with experiment requires the identification the electronic transitions to which the peaks in our calculated absorption spectra correspond. In Casida’s approach information about electronic transitions is inherently produced, while in RT-TDDFT it is not.

It is often possible to identify the corresponding transition by examining the polarisation and energy of peaks and comparing to that of optically allowed transitions experimentally. Where possible, in order to more confidently assign peaks of our calculated absorption spectra to particular electronic transitions, we have followed the procedure in²⁶ whereby a sinusoidal electric field

tuned to a particular excitation mode is applied. A resulting electronic resonance is set up, allowing us to examine the difference between ground state charge density and excited state charge density and thereby infer the electronic transition (details and example results for the first transitions of the CO and C₂H₄ molecules can be found in supporting information SI3).

2.2.1 Basis Sets

Our support functions are expanded in a basis of numerical orbitals, in this case pseudo-atomic orbitals generated within the Siesta code²⁷. These PAOs are eigenfunctions of the atomic pseudopotentials with a confinement energy shift used to determine a radial cut-off for the orbitals, beyond which they are zero. This confinement energy provides a single parameter to define the cut off radii for different orbitals, and is the energy each orbital obtains on being confined by an infinite potential to a particular radius. It is clear that a minimal basis with which ground state properties are accurately reproduced will generally not be satisfactory for calculating excited state properties, and therefore we illustrate the basis set dependence of two selected transitions for the C₂H₄ molecule.

Multiple orbitals per angular momentum channel can be used (multiple- ζ), with the shape of multiple orbitals determined by a split norm procedure²⁷. This procedure uses a parameter to define the norm of a numerical orbital outside some radius where they match the tail of the first zeta PAO, and within this radius they vary smoothly to the origin. Subtracting this numerical orbital from the original PAO gives the multiple-zeta orbital. Of course it is possible to define these radii by hand and fine tune the basis set. In addition to multiple zeta, polarisation orbitals can be included within the basis set, and are obtained by solving the same atomic pseudo-atomic problem but with an applied electric field.

We use the notation SZ, DZ, 3Z, 4Z to describe single zeta, double zeta, triple zeta and so on. Similarly we describe the number of polarisation orbitals included in the basis by SZP, SZ2P and SZ3P (one, two and three polarised orbitals respectively).

To first gauge the effect of varying our basis set on the results we have performed calculations

Table 1: Basis set dependence of calculated TDLDA transition energies (eV.) for first valence ($\pi \rightarrow \pi^*$) and Rydberg ($\pi \rightarrow 3s$) excitations for the C_2H_4 molecule.

Transition	Basis Set								Ref. ²⁸	Expt. ²⁹
	2ZP	2Z2P	3ZP	3Z2P	4ZP	4Z2P	5ZP	5Z2P		
1 meV										
$\pi \rightarrow \pi^*$	7.84	7.62	7.73	7.62	7.67	7.62	7.67	7.62	7.45	8.0
$\pi \rightarrow 3s$	8.43	7.95	7.78	7.67	7.46	7.40	7.46	7.29	6.69	7.11
5 meV										
$\pi \rightarrow \pi^*$	7.82	7.73	7.75	7.69	7.70	7.68	7.67	7.67	7.45	8.0
$\pi \rightarrow 3s$	10.64	8.03	7.88	7.76	7.57	7.51	7.46	7.45	6.69	7.11

on the ethylene molecule with varying numbers of PAOs and two different confinement energies. The basis sets have been generated with a confinement energy of 1 meV and 5 meV, resulting in confinement radii of 4.93 and 4.24 Å for the carbon atoms respectively, and radii of 4.77 and 4.21 Å for the hydrogen atoms respectively. The total run time was 14.51 fs. (600 au.) with a time step of ~ 0.0242 fs (0.1 au). The results can be seen in table 1.

Calculated energies for the $\pi \rightarrow 3s$ transition show a wide variation with basis set choice, while the $\pi \rightarrow \pi^*$ valence transition varies less. This is in line with expectation, given the more diffuse nature of the Rydberg transition we would expect its description to require larger basis. The effect of systematically increasing the number of basis functions is to improve our results with respect to that of the reference values. Similarly increasing the cut-off radii, by reducing the confinement energy, tends to improve the quality of the result. This is to be expected, as increasing the size of our basis set, while systematically increasing the range, will maximise the variational degrees of freedom available to describe our time dependent density matrix.

However our values are still far from those computed elsewhere, and we find generally that for small molecules it is essential to use a large basis with multiple extended polarisation orbitals in order to produce results in line with other works. In addition we find that fine tuning the radial cut-offs by hand, as opposed to using the confinement energy and split norm procedure, can allow us to improve the quality of our results for small molecules.

2.2.2 Small Molecule Results

Exhibited in table 2 are the calculated transitions for our four test molecules. In the case of the smallest molecules (carbon monoxide, ethylene, and methane) a hand tuned 5Z4P basis set is employed, while for benzene the result is obtained using a 2Z2P basis with a 5meV confinement energy. Also presented in figure 1 are the optical absorption spectra for the benzene and carbon-monoxide molecules, along with the experimental data.

Table 2: Comparison of calculated TDLDA transition energies for small molecules with other values and experiment. Conquest results obtained with 5Z4P basis sets, with the exception of benzene (2Z2P).

Molecule	Transition	RT-TDDFT (eV.)	Ref	Expt
CO	$\sigma \rightarrow \pi^*$	8.17	8.20 ³⁰	8.51 ³¹
CH ₄	$T_2 \rightarrow 3s$	9.22	9.27 ³²	9.70 ³³
C ₂ H ₄	$\pi \rightarrow \pi^*$	7.48	7.45 ³²	8.00 ²⁹
C ₆ H ₆	$\pi \rightarrow \pi^*$	6.87	~ 6.90 ³⁴	6.90 ³⁵

We can see a strong agreement between our results and that of other studies, giving us confidence in our implementation. Very good agreement is exhibited between the calculated benzene absorption spectra and the experimental values using a reasonably modest 2Z2P basis set. This highlights the point that for larger molecules we have generally found that the need for large hand tuned basis sets, as is necessary for the smaller molecules, is reduced. Typically results in agreement with those in the literature and experiment are found using smaller basis sets, a point that is important to bear in mind, given the context of linear scaling methods.

3 Propagator Unitarity

Having demonstrated the correctness of our implementation and explored the influence of basis sets, we now turn to our main concern, the effects of localisation in linear scaling methods on the accuracy of results.

We wish the total charge in our system to remain stable, and in order for this to be the case the

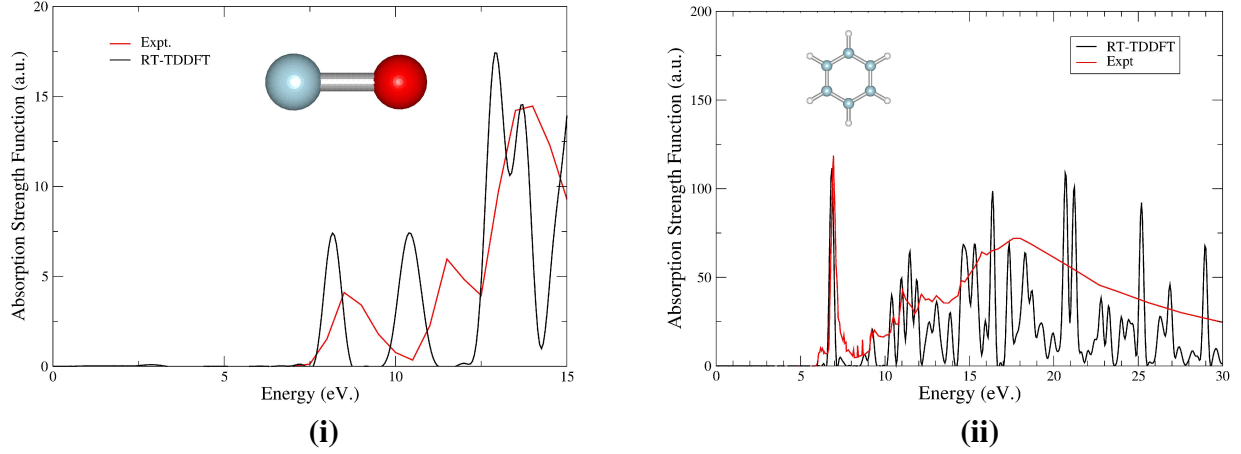


Figure 1: **(i)**: Absorption strength function for carbon monoxide from RT-TDDFT and experiment. Experimental data taken from³¹. **(ii)** Absorption strength function for Benzene from RT-TDDFT. Experimental data taken from³⁵.

propagators must be unitary with respect to non-orthogonal basis set. Conserving total probability, where

$$P(t + \Delta t) = \mathbf{c}^\dagger(t + \Delta t) \mathbf{S} \mathbf{c}(t + \Delta t) \quad (13)$$

$$= \mathbf{c}^\dagger(t) \mathbf{U}^\dagger \mathbf{S} \mathbf{U} \mathbf{c}(t) \quad (14)$$

$$= P(t) \quad (15)$$

we see that in order for the above to be true, and for the total charge to be conserved, the following must hold:

$$\mathbf{U}^\dagger \mathbf{S} \mathbf{U} - \mathbf{S} = 0 \quad (16)$$

where \mathbf{U} is our propagator matrix and \mathbf{S} is the overlap matrix.

From our approximation for the matrix exponential, eq. ??, it can be shown that, if it were exact, our propagators would indeed exhibit this property. However, as it is impossible for us to store an infinite sum on our computer, we must truncate our Taylor expansion at some point. Doing so will introduce errors, with two factors affecting the scale of the break from S-unitarity; the time

step and the number of terms in our summation. While we can extend our expansion arbitrarily, and reduce the time step arbitrarily, we wish to avoid excess computational expense by keeping the expansion as small as possible and the time step as large as possible within some acceptable margin of accuracy. We can directly examine the unitarity of our propagators through equation ??.

3.1 Time-Step Dependence

As a test we have examined the extent of the break from unitarity for a range of time-steps and number of terms in the matrix exponential expansion. We have used a small molecule for the purpose, benzene, with a small applied electric field perturbation with a Gaussian profile centered on $t = 0$.

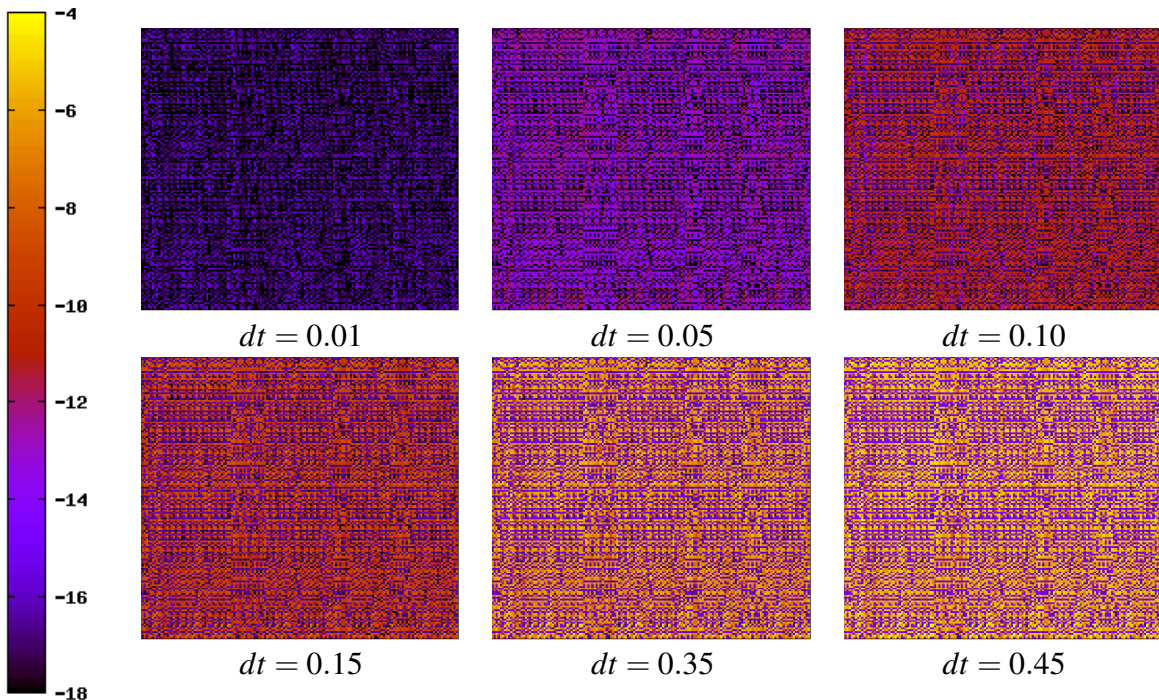


Figure 2: Plot of the absolute values of matrix $\mathbf{U}^\dagger \mathbf{S} \mathbf{U} - \mathbf{S}$ (on a base 10 log scale), illustrating the propagator unitarity for the exponential midpoint propagator, for varying time step sizes (in a.u.). The system studied is a single benzene molecule, and the matrix is shown at the end of a 10 a.u. run.

Exhibited in figure 2 we can see the dependence on simulation time step of the propagator unitarity, with the obvious trend being that as the time step is reduced the propagator approaches

unitarity. We can see that even for time steps up to ~ 0.15 a.u. the propagator maintains its unitarity to a high degree (similar results were obtained for each of the propagators). The corresponding effect on the charge conservation can be seen in figure 3 and, as expected we see that as the time step increases the conservation of charge deteriorates with the propagation eventually becoming unstable for large timesteps. While the maximum permissible timestep will depend on the system under study, we found that generally a timestep of 0.06 a.u. or below provided satisfactory charge conservation.

The form of our propagators (see supp. info.) requires the extrapolation of the Hamiltonian matrix to some unknown point beyond the current time t , \mathbf{H}_+ . As suggested by Marques et al.²⁴ in order to minimise errors it is possible to carry this procedure out self-consistently. In our case meaning that we propagate $\mathbf{K}(t)$ to $\mathbf{K}(t + \Delta t)$ based on an extrapolated Hamiltonian. We then construct a new Hamiltonian matrix $\mathbf{H}(t + \Delta t)$ using $\mathbf{K}(t + \Delta t)$. \mathbf{H}_+ can then be interpolated from Hamiltonian matrices for times up to and including $(t + \Delta t)$, and the whole procedure is iterated until some self-consistency criteria is obtained. Generally speaking this procedure is performed three times in the early stages of a run, following a perturbation, and reduces to two as the run progresses. The effect of not performing this self-consistency procedure on the charge conservation can be seen in figure 3. While the self-consistency cycle is found to improve the charge conservation, in reality for small time steps the difference in charge conservation and calculated properties is not found to be significant enough to warrant the extra computational load of constructing the Hamiltonian matrix several times per time-step. As a compromise we enforce the self-consistency only for a small number of steps ($\sim 50 - 100$) at the beginning of a run, typically when our external electric field is applied for the study of the linear response and the external perturbation is largest.

A significant point to note is that little difference is exhibited between the calculated results using each of the three propagators in terms of charge conservation, and in general we have found this to be the case. It is reported that for systems with strongly time-dependent Hamiltonians the fourth order Magnus propagator, \mathbf{U}_{M4} , is advantageous²⁴, but for our present work this is not the case and we have opted for the simplest exponential midpoint propagator throughout.

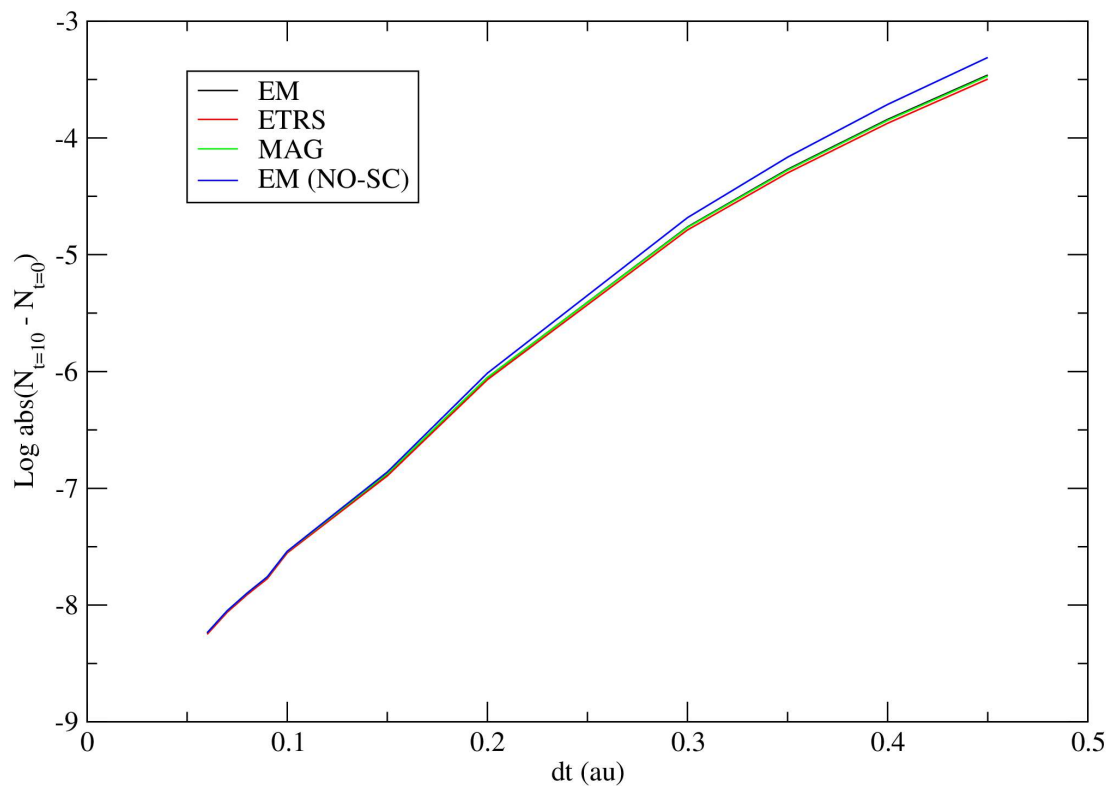


Figure 3: Variation in total charge (on a base 10 log scale) with time step size, following a 10 au. run for benzene using all three propagators. Also included is charge variation for the EM propagator without the self-consistent propagator step (see text for details).

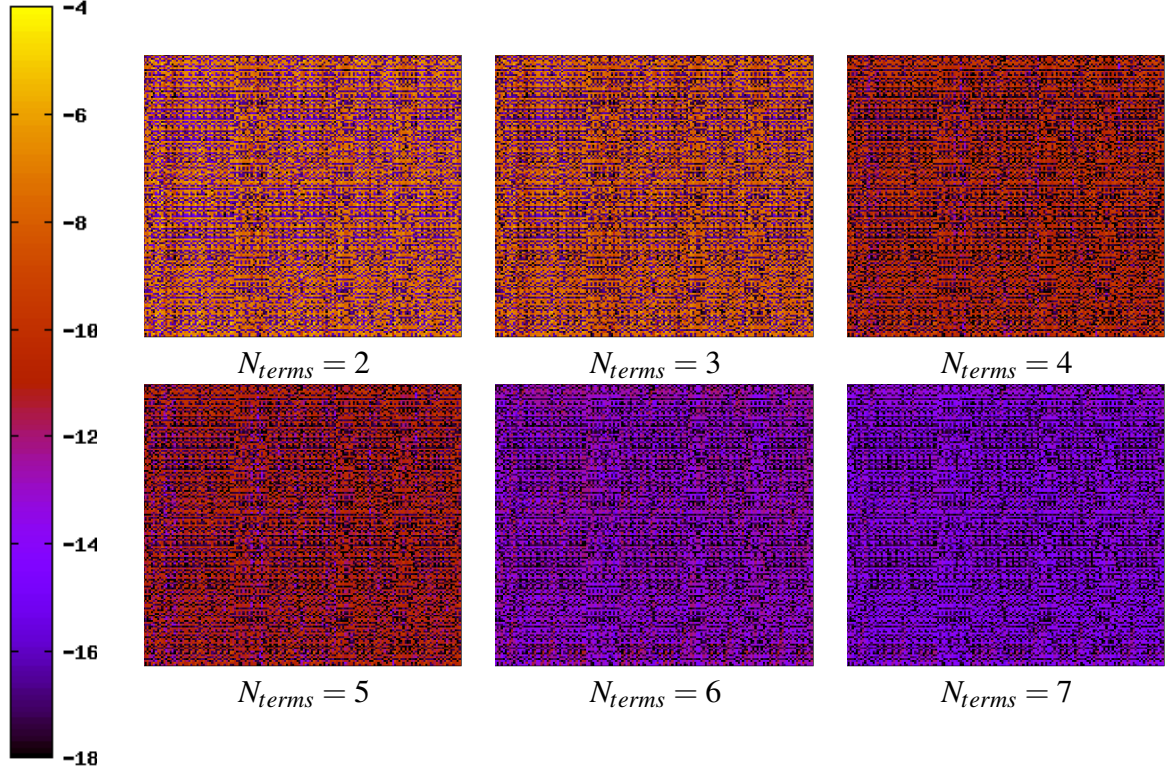


Figure 4: Plot of the absolute values of the matrix $\mathbf{U}^\dagger \mathbf{S} \mathbf{U} - \mathbf{S}$ (on a base 10 log scale), illustrating the propagator unitarity for the exponential midpoint propagator, for differing number of terms in the Taylor expansion for our propagator. The system studied is a single benzene molecule, and the matrix is shown at the end of a 10 au. run ($dt = 0.04$ au.)

3.2 Matrix Exponential Truncation

The effect of truncating the Taylor expansion used to evaluate the matrix exponential on the unitarity of the propagator can be seen in figure 4. We see that reducing the number of terms reduces the unitarity of the propagator, as expected. Looking at figure 5 the convergence of the charge conservation with the number of terms in the exponential expansion can be seen. We find that we reach good convergence with six terms included in the expansion, and we opt for this level of accuracy throughout the remainder of the paper.

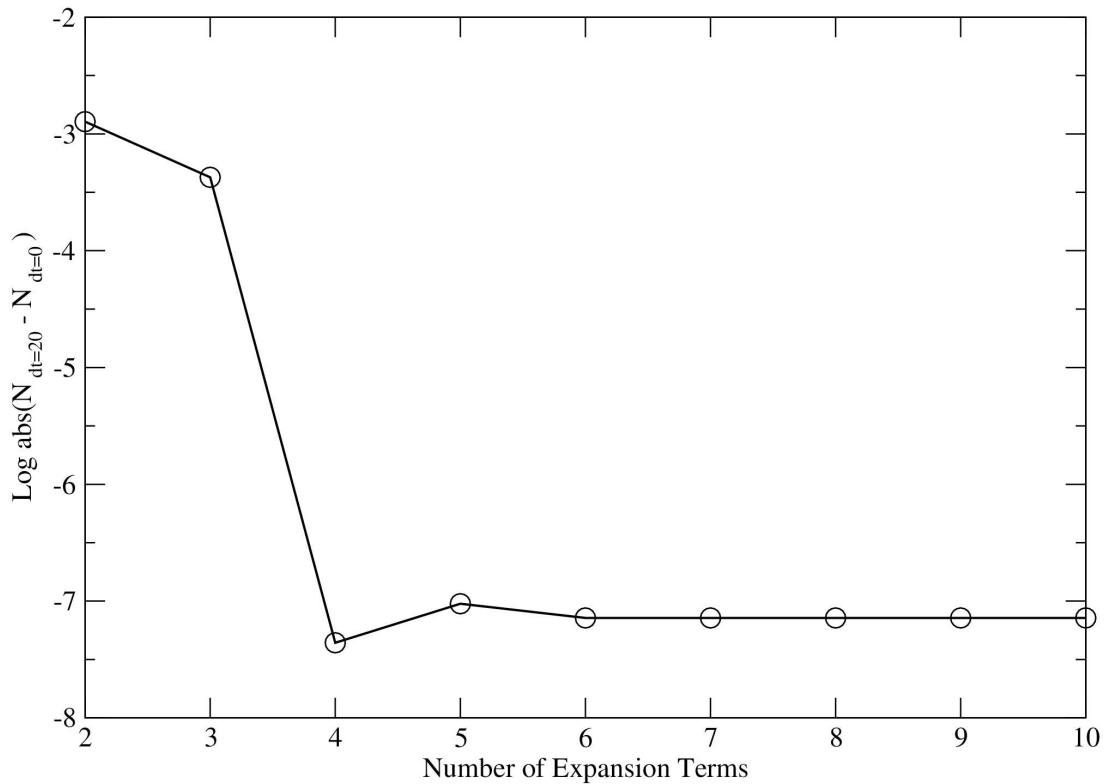


Figure 5: Absolute variation in total charge (on a base 10 log scale) with the number of terms in our matrix exponential expansion, following a 20 au. run for benzene using the EM propagator with a time step of 0.04 au.

4 Alkane Molecules: Testing Matrix Truncation Effects

In this section we perform calculations on long chain alkane molecules, an example of which can be seen in figure 6 ($C_{11}H_{24}$) along with the general chemical structure for an alkane chain. Our aim is to examine the effect of matrix truncation on the propagation of the density matrix and propagator unitarity, along with the computational scaling with system size.

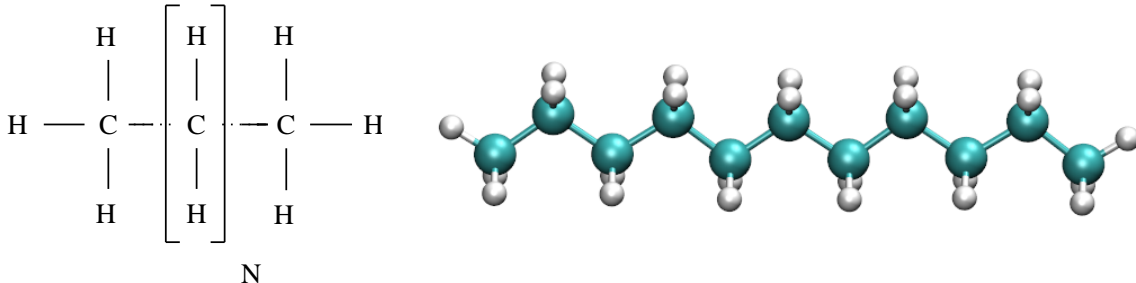


Figure 6: Alkane molecule chemical structure (left) and the molecular structure of the $C_{11}H_{24}$ molecule (right).

As a first step we calculate the absorption spectra for the $C_{11}H_{24}$ molecule for several different basis sets using the generalised gradient PBE functional³⁶ (all further calculations in this section are performed with this functional), and the results can be seen in figure 7. Experimentally as the length of the alkane carbon chain increases, the absorption onset is found to reduce, and the reported adsorption onset for $C_{10}H_{22}$ is ~ 175 nm.³⁷ (~ 7.1 eV.). We see that as the number of PAOs in the basis set is increased the calculated absorption onset approaches this value. Particularly noticeable is the change of the absorption energy caused by the addition of polarisation orbitals. Similarly a significant shift is induced by extending the range of the PAOs (a variation from 55 meV to 25 meV in the confinement energy extends the radii of the carbon and hydrogen basis sets by ~ 0.35 Å and 0.33 Å respectively). This is understandable, given that the first transitions in the alkane molecules are reported as being Rydberg in character³⁷, we would expect the addition of more diffuse PAOs to improve the description of these excitations. Given the well documented difficulties of TDDFT to accurately describe Rydberg transitions³⁸, and given that this is not our aim in any case, we proceed to carry out our tests with the SZP and SZ2P basis sets generated

using a confinement energy of 55meV (radial cut off for the PAOs is 3.31Å and 3.12Å for carbon and hydrogen respectively).

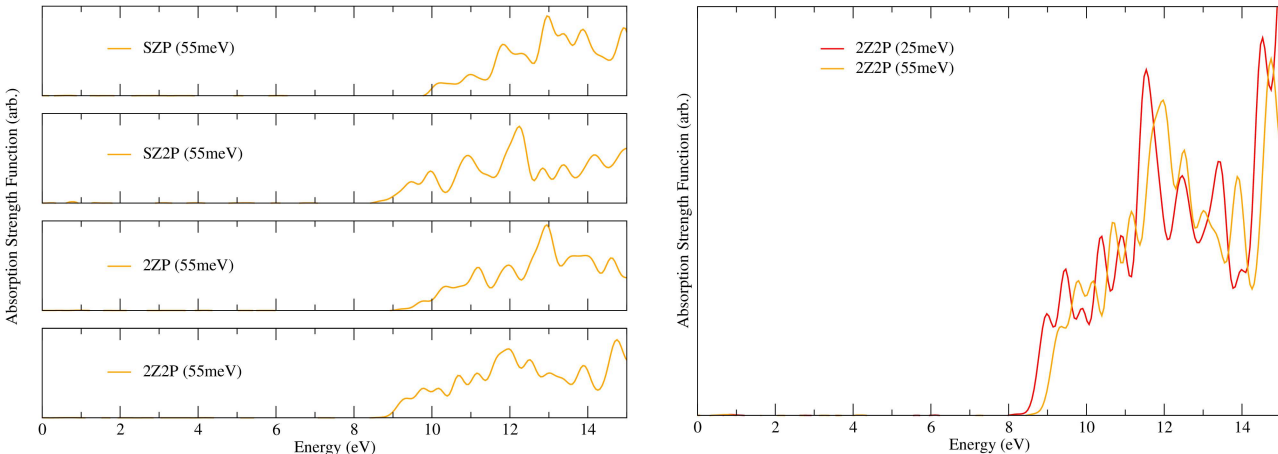


Figure 7: Basis set variation of the calculated alkane optical absorption spectra. Effect of increasing the number of PAOs in the basis set(left) and the effect of extending the radii of the basis functions(right) are shown.

It is worth noting that several previous works have been done on linear scaling TDDFT (for a review see²¹). Our approach closely resembles that of Chen et. al.^{10–14}. Indeed Chen et al. have previously studied the long chain alkanes within the linear scaling excited state regime²², calculating the absorption onset at around 8 eV for $C_{40}H_{82}$ with the LDA functional.

4.1 Propagator Truncation

The use of a basis of non-orthogonal atomic orbitals requires the inverse overlap matrix for our propagation (indeed this matrix is required for ground state calculations in any case), as seen in equation ???. In order to compute the inverse overlap matrix Conquest uses Hotelling’s method³⁹, however for poorly conditioned overlap matrices computing the inverse overlap matrix can prove difficult. In our current implementation of TDDFT the atoms remain stationary and so too, therefore, does the overlap matrix. Therefore we have also included the possibility of computing the inverse overlap with the SCALAPACK routines. Although the scaling will not be linear, comput-

ing the inverse overlap in this way makes only a relatively small contribution to our total TDDFT runtime, as we only calculate the inverse overlap once at $t = 0$.

While it is apparent that the overlap matrix will be sparse, allowing it to be truncated, the inverse of a sparse matrix will not in general be sparse itself. We have therefore tested the effect of truncating both the \mathbf{S}^{-1} matrix and the $\mathbf{S}^{-1}\mathbf{H}$ matrix on the propagation. Figure 8 shows the average absolute error in the matrix elements of \mathbf{S}^{-1} and the $\mathbf{S}^{-1}\mathbf{H}$ matrices caused by truncation (the error in \mathbf{S}^{-1} elements given is the average of the elements of the $\mathbf{S}^{-1}\mathbf{S}-\mathbf{I}$ matrix, and the error in the $\mathbf{S}^{-1}\mathbf{H}$ is calculated with the values from an untruncated \mathbf{S}^{-1} matrix).

As the range of the matrices increases the error caused by the truncation converges towards zero, as we expect. The \mathbf{S}^{-1} matrix converges less quickly than the $\mathbf{S}^{-1}\mathbf{H}$ matrix, indicating that it is more dense than the $\mathbf{S}^{-1}\mathbf{H}$ matrix. The effect truncation of these matrices has on the unitarity of the propagators can be seen in figure 9. We see that the unitarity converges as the $\mathbf{S}^{-1}\mathbf{H}$ range increases, and the propagators are converged with a range of around ~ 22.5 -27.5 Bohr. This indicates that the $\mathbf{S}^{-1}\mathbf{H}$ matrix is indeed sparse, and we can safely truncate it. Similarly it makes sense to truncate the \mathbf{S}^{-1} matrix, given that we are truncating $\mathbf{S}^{-1}\mathbf{H}$ and that the Hamiltonian matrix is sparse. We can see this by noting that the unitarity of the propagator in figure 9 is also well converged for each of the truncation ranges imposed on the inverse overlap.

As additional atoms are added the Hamiltonian matrix, overlap matrix, and the inverse overlap will vary. Increasing the system size may therefore affect the ranges of these matrices. We have tested this effect by fixing the \mathbf{S}^{-1} and $\mathbf{S}^{-1}\mathbf{H}$ ranges at 30 and 35 Bohr respectively, and examined the error in the truncated $\mathbf{S}^{-1}\mathbf{H}$ matrix with system size with the results shown in figure 10. We see that the error changes slightly on increasing system size, but converges as the size increases. Consequently the propagator unitarity was found to exhibit the same trend. This illustrates that the $\mathbf{S}^{-1}\mathbf{H}$ is well ranged, irrespective of system size, allowing us to impose a cut-off radii on both of these matrices. In effect this ensures that as the system size increases, the computational load can be made to scale linearly.

Similarly, increasing the number of basis functions will directly affect the overlap matrix, and

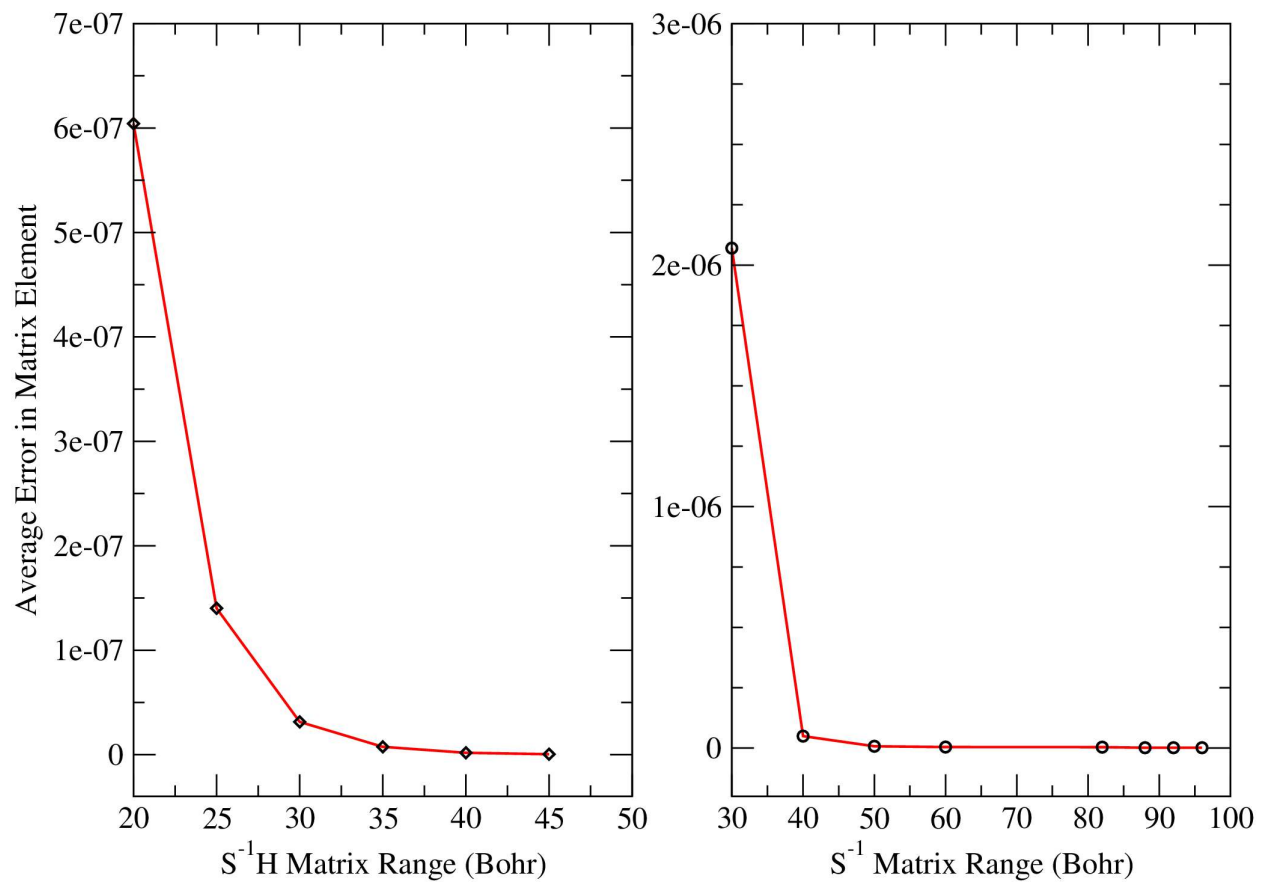


Figure 8: Average absolute error in the $\mathbf{S}^{-1}\mathbf{H}$ (left) and \mathbf{S}^{-1} (right) matrix elements with matrix range for the $\text{C}_{47}\text{H}_{96}$ molecule. SZP basis set is used, generated with a 55meV confinement potential.

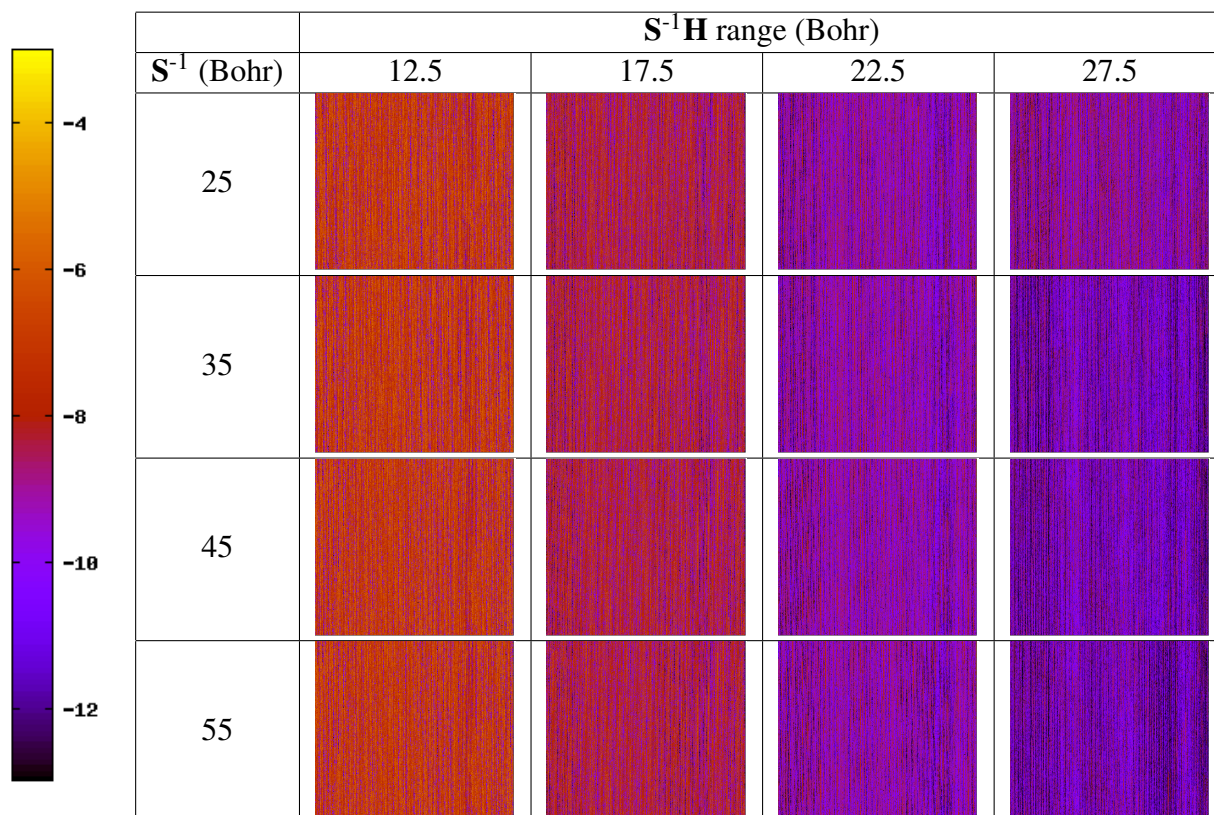


Figure 9: Plot of the absolute values of the matrix $\mathbf{U}^\dagger \mathbf{S} \mathbf{U} - \mathbf{S}$ (on a base 10 log scale), illustrating the propagator unitarity for differing truncation ranges of the \mathbf{S}^{-1} and $\mathbf{S}^{-1}\mathbf{H}$ matrices for the $\text{C}_{47}\text{H}_{96}$ molecule

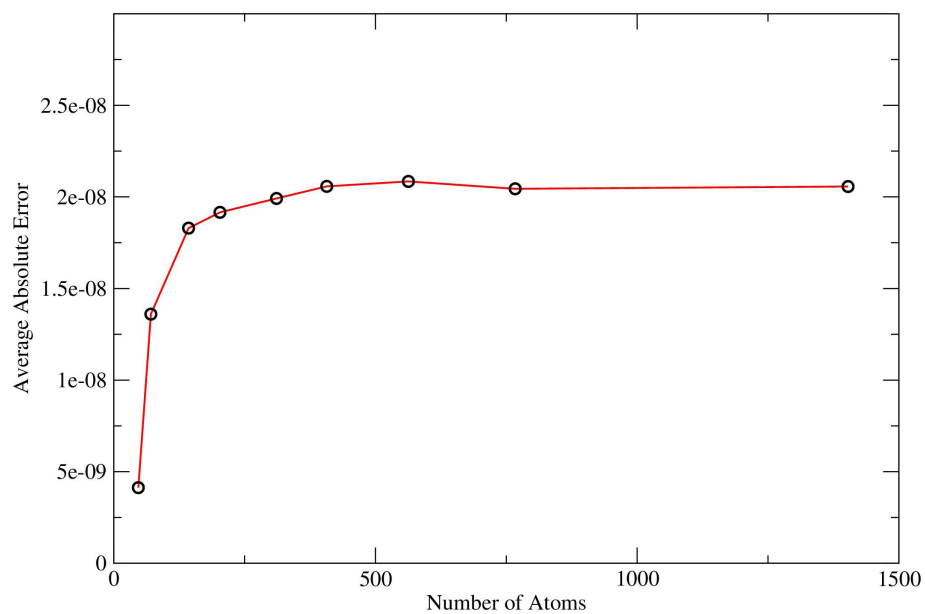


Figure 10: Average absolute error in the $\mathbf{S}^{-1}\mathbf{H}$ matrix elements with system size.

consequently the inverse overlap and the propagator. In order to gauge the extent of this effect we have examined the $C_{103}H_{208}$ molecule with a larger basis set (SZ2P as opposed to SZP). Exhibited in figure 11 is the absolute value of the $U^\dagger S U - S$ matrix with $S^{-1}H$ matrix truncation range. Despite the larger number of basis set functions we see that the $S^{-1}H$ matrix is still well ranged, although the range is wider when compared to the SZP results of figure 9, and again a truncation will lead to a computational load that scales linearly with system size.

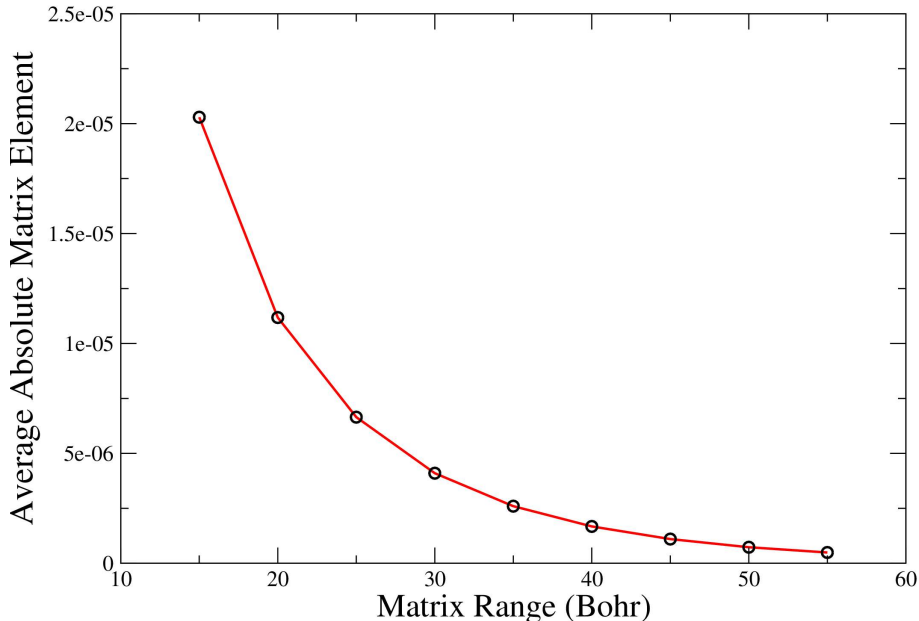


Figure 11: Average value of the $U^\dagger S U - S$ matrix with $S^{-1}H$ matrix range for the $C_{103}H_{208}$ molecule calculated with a SZ2P basis set.

A further point to note is that it is possible to avoid the use of the inverse overlap matrix in the TDDFT propagation altogether. Chen et al. have employed a Cholesky orthogonalisation scheme to bypass the need for the inverse overlap²². However using this scheme requires the inverse of the Cholesky decomposition, and it is not apparent that it will be more sparse than the inverse overlap. It is possible that this scheme might improve the calculation of the propagator, as the orthogonalised Hamiltonian may be more localised than our $S^{-1}H$ matrix. Calculating the

Cholesky decomposition can be made to scale linearly, and implementation of this alternative method has already begun in order to contrast the two approaches. However this method cannot be easily transferred to periodic cells given the Conquest matrix storage, and inversion remains important.

4.2 Density Matrix Truncation and Scaling

Finally we examine the effect of truncating the density matrix, and have performed calculations generating spectra for the $C_{47}H_{96}$ molecule at varying truncation radii, R_{Cut} , of the density matrix. Typically for ground state calculations a suitable typical density matrix truncation range is around 16-20 Bohr. The results can be seen in figure 12, and generally we find that as the density matrix cut-off increases the spectra tend to converge, as expected, with higher lying states requiring a larger cut-off to converge. We can see from the comparison of $R_{Cut} = 30$ and $R_{Cut} = 35$ that there is good agreement for the initial transitions, as well as the general shape of the spectra.

Applying this $R_{Cut} = 35$ Bohr cut-off (along with a cut off of 35 Bohr. on the $\mathbf{S}^{-1}\mathbf{H}$ matrix) we can examine the computational scaling with system size, with the results exhibited in figure 13.

5 Conclusions

We have outlined our implementation of real-time time dependent density functional theory in the Conquest $\mathcal{O}(N)$ code. We have demonstrated the soundness of the implementation through benchmark tests for small molecules, and also discussed the effect of basis set and system sizes on the results.

$\mathcal{O}(N)$ approaches utilise the density matrix, as opposed to working directly with Kohn-Sham orbitals, providing a route to the linear scaling computational time with system size by its truncation. We have discussed the range of our propagator matrices for an alkane chain test system, and the implications of this matrix truncation on the unitarity of the propagation. Similarly we have examined the effect of truncating the density matrix on the calculated optical absorption spectra,

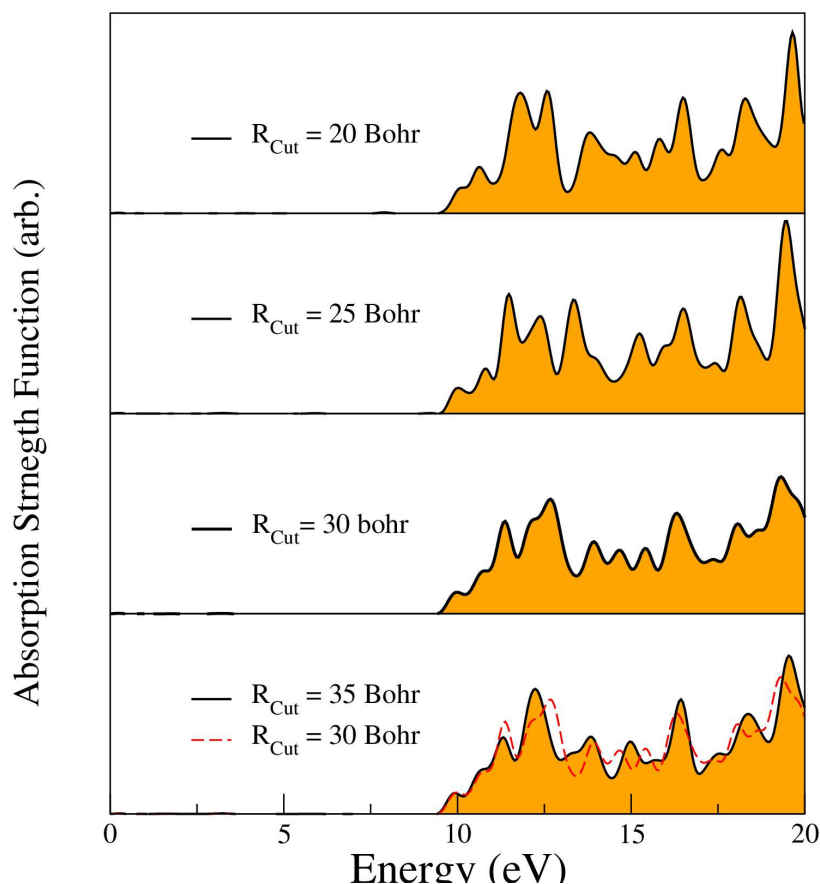


Figure 12: K matrix truncation radii dependence: Spectra generated for the $C_{47}H_{96}$ molecule at varying density matrix cut-off radii. (Total run time of 400 a.u. at a time step of 0.05 a.u.)

showing that the range required is much more extended than that required for converged ground state properties. Nevertheless, we have shown that accurate linear scaling TDDFT calculations are practical. While the impact of localisation cut-off in the charge density matrix on these TDDFT calculations is a topic warranting further study, we have shown that in truncating these matrices at a suitable point we obtain a computational load that increases linearly with system size. This offers a complementary approach to the usual Casida linear response approach: linear response TDDFT is well suited to relatively small systems, while linear scaling RT-TDDFT offers a viable method for studying excitations in large systems. We have shown linear scaling beyond 1,000 atoms, and 10,000+ atoms are perfectly practical with the excellent parallel scaling available in Conquest.

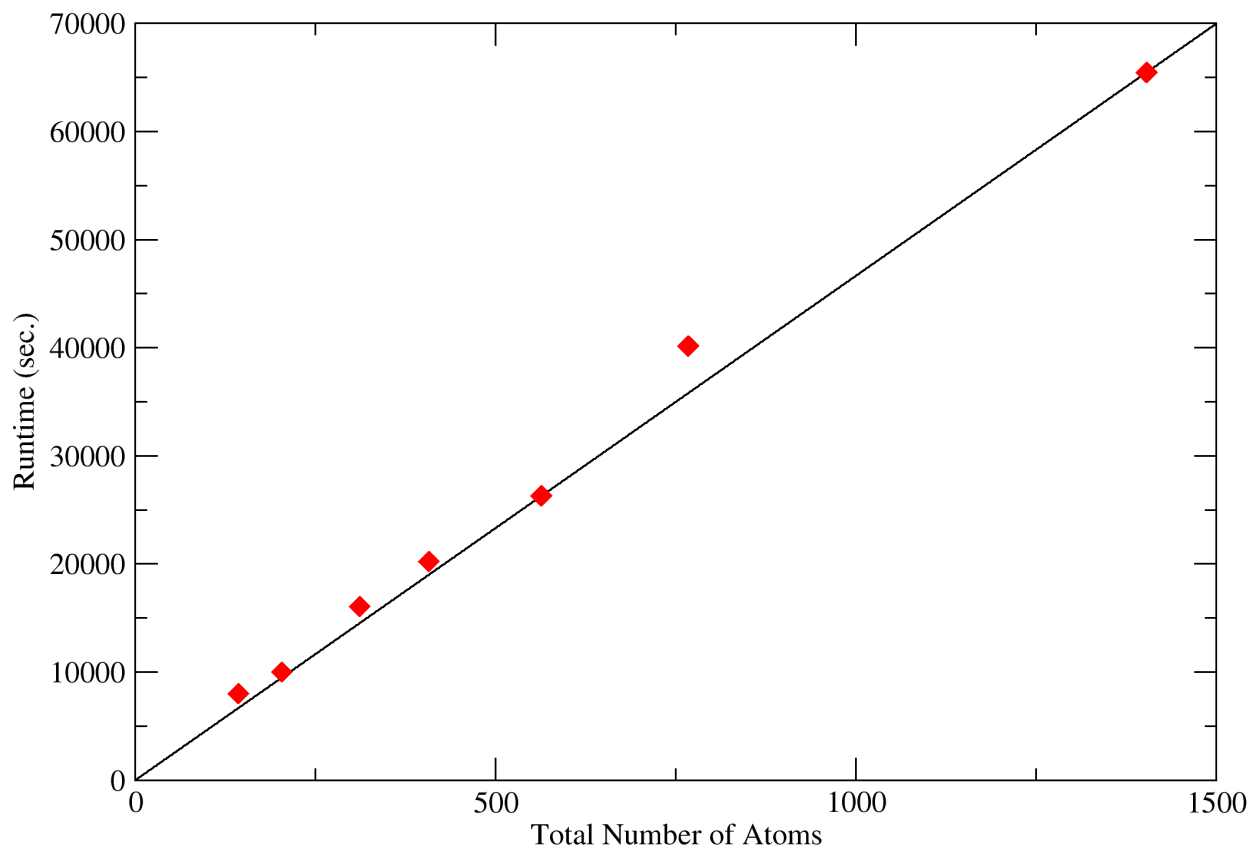


Figure 13: Computational TDDFT run time versus system size for long chain alkane molecules. The system was run with a timestep of 0.05 a.u. for a total time of 10 a.u.

Supporting Information

Details of the propagators used, the calculation of the linear response (with benzene as an example) and the method employed for identifying transitions (with CO and C₂H₄ as examples) can be found in supporting information. This material is available free of charge via the Internet at <http://pubs.acs.org>.

Acknowledgements

C.O'R. is supported by the MANA-WPI project. This work made use of the facilities of HECToR, the UK's national high-performance computing service, which is provided by UoE HPCx Ltd at the University of Edinburgh, Cray Inc and NAG Ltd, and funded by the Office of Science and Technology through EPSRC's High End Computing Programme. Calculations were performed at HECToR & ARCHER through the UKCP Consortium. The authors acknowledge the use of the UCL Legion High Performance Computing Facility, and associated support services, in the completion of this work.

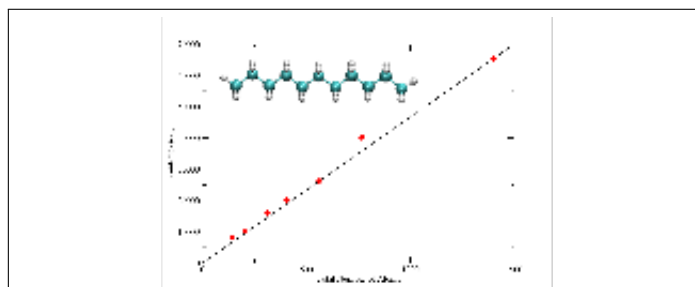
References

- (1) Hohenberg, P.; Kohn, W. *Phys. Rev.* **1964**, *136*, B864–B871.
- (2) Kohn, W.; Sham, L. J. *Phys. Rev.* **1965**, *140*, A1133–A1138.
- (3) Runge, E.; Gross, E. K. U. *Phys. Rev. Lett.* **1984**, *52*, 997–1000.
- (4) Gross, E. K. U.; Kohn, W. *Phys. Rev. Lett.* **1985**, *55*, 2850–2852.
- (5) Casida, M. E. in *Recent Advances in Density Functional Methods, Part I*, edited by D.P. Chong **1995**, 155.
- (6) Kronik, L.; Makmal, A.; Tiago, M. L.; Alemany, M. M. G.; Jain, M.; Huang, X.; Saad, Y.; Chelikowsky, J. R. *physica status solidi (b)* **2006**, *243*, 1063–1079.
- (7) Rocca, D.; Gebauer, R.; Saad, Y.; Baroni, S. *The Journal of Chemical Physics* **2008**, *128*, –.
- (8) Yabana, K.; Bertsch, G. F. *Phys. Rev. B* **1996**, *54*, 4484–4487.
- (9) Bowler, D. R.; Miyazaki, T. *Reports on Progress in Physics* **2012**, *75*, 036503.
- (10) Yokojima, S.; Chen, G. *Chemical Physics Letters* **1998**, *292*, 379 – 383.
- (11) Yokojima, S.; Chen, G. *Phys. Rev. B* **1999**, *59*, 7259–7262.

- (12) Yokojima, S.; Chen, G. *Chemical Physics Letters* **1999**, *300*, 540 – 544.
- (13) Yokojima, S.; Zhou, D.; Chen, G. *Chemical Physics Letters* **1999**, *302*, 495 – 498.
- (14) Liang, W.; Yokojima, S.; Chen, G. *The Journal of Chemical Physics* **1999**, *110*, 1844–1855.
- (15) Liang, W.; Yokojima, S.; Zhou, D.; Chen, G. *The Journal of Physical Chemistry A* **2000**, *104*, 2445–2453.
- (16) Tsolakidis, A.; Sánchez-Portal, D.; Martin, R. M. *Phys. Rev. B* **2002**, *66*, 235416.
- (17) Zuehlsdorff, T. J.; Hine, N. D. M.; Spencer, J. S.; Harrison, N. M.; Riley, D. J.; Haynes, P. D. *The Journal of Chemical Physics* **2013**, *139*, –.
- (18) Prodan, E.; Kohn, W. *Proceedings of the National Academy of Sciences of the United States of America* **2005**, *102*, 11635–11638.
- (19) Goringe, C.; Hernández, E.; Gillan, M.; Bush, I. *Computer Physics Communications* **1997**, *102*, 1 – 16.
- (20) Bowler, D. R.; Miyazaki, T. *Journal of Physics: Condensed Matter* **2010**, *22*, 074207.
- (21) Yam, C.; Zhang, Q.; Wang, F.; Chen, G. *Chem. Soc. Rev.* **2012**, *41*, 3821–3838.
- (22) Yam, C.; Yokojima, S.; Chen, G. *Phys. Rev. B* **2003**, *68*, 153105.
- (23) Moore, G. *Linear Algebra and its Applications* **2011**, *435*, 537 – 559.
- (24) Castro, A.; Marques, M. A. L.; Rubio, A. *The Journal of Chemical Physics* **2004**, *121*, 3425–3433.
- (25) Tsolakidis, A.; Sánchez-Portal, D.; Martin, R. M. *Phys. Rev. B* **2002**, *66*, 235416.
- (26) Min, S. K.; Cho, Y.; Kim, K. S. *The Journal of Chemical Physics* **2011**, *135*, 244112.
- (27) Soler, J. M.; Artacho, E.; Gale, J. D.; García, A.; Junquera, J.; Ordejón, P.; Sánchez-Portal, D. *Journal of Physics: Condensed Matter* **2002**, *14*, 2745.

- (28) Matsuzawa, N. N.; Ishitani, A.; Dixon, D. A.; Uda, T. *The Journal of Physical Chemistry A* **2001**, *105*, 4953–4962.
- (29) Hammond, V. J.; Price, W. C. *Trans. Faraday Soc.* **1955**, *51*, 605–610.
- (30) Hu, C.; Sugino, O.; Miyamoto, Y. *Phys. Rev. A* **2006**, *74*, 032508.
- (31) Chan, W.; Cooper, G.; Brion, C. *Chemical Physics* **1993**, *170*, 123 – 138.
- (32) Matsuzawa, N. N.; Ishitani, A.; Dixon, D. A.; Uda, T. *The Journal of Physical Chemistry A* **2001**, *105*, 4953–4962.
- (33) Curtis, M. G.; Walker, I. C. *J. Chem. Soc., Faraday Trans. 2* **1989**, *85*, 659–670.
- (34) Yabana, K.; Bertsch, G. F. *International Journal of Quantum Chemistry* **1999**, *75*, 55–66.
- (35) Koch, E.; Otto, A. *Chemical Physics Letters* **1972**, *12*, 476 – 480.
- (36) Perdew, J. P.; Burke, K.; Ernzerhof, M. *Phys. Rev. Lett.* **1996**, *77*, 3865–3868.
- (37) Costner, E. A.; Long, B. K.; Navar, C.; Jockusch, S.; Lei, X.; Zimmerman, P.; Campion, A.; Turro, N. J.; Willson, C. G. *The Journal of Physical Chemistry A* **2009**, *113*, 9337–9347, PMID: 19630422.
- (38) Casida, M. E.; Jamorski, C.; Casida, K. C.; Salahub, D. R. *The Journal of Chemical Physics* **1998**, *108*, 4439–4449.
- (39) Palser, A. H. R.; Manolopoulos, D. E. *Phys. Rev. B* **1998**, *58*, 12704–12711.

Graphical TOC Entry



Linear scaling TDDFT: run time versus system size for long chain alkane molecules.